

# Modeling for fingering patterns with an assembly of splitting elements

So Kitsunezaki

Department of Physics, Graduate School of Sciences,  
Kyoto University, Kyoto 606, Japan

July 31, 1999

## Abstract

For the purpose of understanding fingering patterns, we propose a simple model system composed of splitting elements where we regard a tip of each finger as a basic dynamical unit. Numerical simulations of the model reproduce turbulent states, fractal and tree-like structures and spatiotemporal intermittency which are all quite similar in behavior to real systems.

keywords: fingering patterns, splitting elements, turbulence, fractal, spatiotemporal intermittency

PACS. 05.40.+j - Fluctuation phenomena, random processes, and Brownian motion

PACS. 05.45.+b - Theory and models of chaotic systems

PACS. 68.70.+w - Whiskers and dendrites

PACS. 87.10.+e - General, theoretical, and mathematical biophysics

e-mail address: kitsune@ton.scphys.kyoto-u.ac.jp

# 1 Introduction

Fingering patterns appear in various systems such as crystal growth[10, 15], viscous fingering[2], electro-deposition[7, 17] and bacterial colonies[11]. In their formation, the fingers repeat growths and splittings, and their movement produces many complicated patterns. They are classified into diffusion-limited aggregation(DLA)[19], dense branching morphology(DBM) and dendritic growth [7, 8, 10, 13, 17] according to their fractal dimension and the appearances of the branches. Recent experiments on directional viscous fingering[1, 12, 14] also report other patterns such as spatio-temporal chaos and spatio-temporal intermittency(STI) and they are similar to those obtained from partial-differential-equation models and coupled map lattices[9].

The above-listed systems are very different microscopically, although in some cases, e.g, the case of bacterial colonies[3, 18], the underlying mechanisms remain unknown. Many models have been proposed to clarify the mechanisms behind each of these systems. When the patterns are seen at a macroscopic level, however, the natures of the fingers seems rather simple and universal: The fingers interact repulsively through a diffusive or a Laplacian field and mutually suppress the growth. Outgrown fingers split into smaller ones. Thus, the variety of fingering patterns seem to come from the complexity of the dynamics of the fingers rather than the differences in their microscopic mechanisms. Therefore, we are concerned with the relationship between the nature of the individual fingers and their dynamics as an assembly[16].

Usually, the fingering pattern grows only in the tip region of the fingers, so that the growth processes may be visualized as trajectories of the tips. Consequently, if we regard each tip as a basic unit, we have a dynamical systems composed of splitting elements. In section 2, we propose a simple phenomenological model in which the tip of each growing finger stays on a straight line, which is consistent with experimental observations on directional fingering and DBM. Our model reproduces patterns similar to real systems in spite of its extreme simplicity. We carried out mathematical analysis and numerical simulations for the simplest version of the model. The types of behavior discovered include turbulent states, fractal-like and tree-like structures discussed in section 3, and also STI discussed in section 4.

## 2 Model

In most systems, the fingers interact through a certain field which obey a simple equation. Therefore, we first consider the form of the interaction at first.

Suppose that the tip region of each finger is sufficiently localized as compared with the distance between neighboring fingers. This is actually the case in many systems, and is best exemplified by some bacterial colonies[6, 13]. Therefore, we will take in the present paper the system of bacterial colony as a target system of our consideration.

The most important factor in the growth of a bacterial colony is considered to be the nutrient concentration  $n(x, y, t)$ . This quantity is assumed to obey a diffusion equation with a consumption term[18],

$$\partial_t n = D \Delta n - \nu n b, \quad (1)$$

where  $D$  is a diffusion constant, and the initial condition  $n(x, y, 0) = n_0$  will be imposed.  $b(x, y, t)$  denotes the density of active bacteria and  $n_0$  and  $\nu$  are constants.  $b(x, y, t)$  is assumed nonvanishing only at the tip of fingers, because the rapid decay of nutrient in the presence of active bacteria will soon make the latter inactive in the inner region of the fingers.

By means of the transformation  $n(\mathbf{x}, t) = n_0 e^{-u(\mathbf{x}, t)}$ , Eq.(1) is rewritten in the form

$$\partial_t u = D(\Delta u - |\nabla u|^2) + \nu b \quad (2)$$

for which the initial condition  $u(x, y, 0) = 0$  is assumed. For  $N$  growing fingers, we have  $N$  tips where the bacterial density is nonvanishing. Therefore, it is convenient to write

$$b(\mathbf{x}, t) \equiv \sum_{i=1}^N b_i(\mathbf{x}, t), \quad b_i(\mathbf{x}, t) = 0 \text{ except in the } i\text{-th tip.}$$

Consider the solution  $u_i(\mathbf{x}, t)$  of the equation

$$\partial_t u_i = D(\Delta u_i - |\nabla u_i|^2) + \nu b_i \quad (3)$$

with the initial condition  $u_i(x, y, 0) = 0$ , where  $b$  in Eq.(2) has been replaced by  $b_i$ .

As discussed in Appendix A, if the tip region of each finger is sufficiently localized, the fields  $u_i(\mathbf{x}, t)$  are so small that  $u(\mathbf{x}, t)$  may be approximated

by their superposition except near the tips. Therefore, the nutrient concentration is represented near the  $i$ -th tip in the form

$$n(\mathbf{x}, t) = n_0 e^{-u(\mathbf{x}, t)} \simeq n_i(\mathbf{x}, t)(1 - U_i(\mathbf{x}, t)), \quad (4)$$

where  $n_i \equiv n_0 e^{-u_i}$  and  $U_i \equiv \sum_{j \neq i} u_j \ll 1$ . The field  $u_i(\mathbf{x}, t)$  is approximated far from the tip in the form

$$u_i(\mathbf{x}, t) \simeq \int_0^\infty dt' G(\mathbf{x} - \mathbf{x}_i(t'), t - t') C_i(t'), \quad (5)$$

where

$$C_i(t) = \frac{1}{n_0} \int d\mathbf{x} \nu n_i(\mathbf{x}, t) b_i(\mathbf{x}, t), \quad \mathbf{x}_i(t) = \frac{1}{n_0 C_i(t)} \int d\mathbf{x} \mathbf{x} \nu n_i(\mathbf{x}, t) b_i(\mathbf{x}, t)$$

and  $G(\mathbf{x}, t)$  is the Green function of a two-dimensional diffusion equation vanishing at infinity, i.e.,  $G(\mathbf{x}, t) = \frac{1}{4\pi Dt} e^{-x^2/4Dt}$ . We call  $C_i$  the mass of the  $i$ -th finger.

We now consider a simple situation that the tip of each growing finger moves alongside with approximately a constant speed like  $y_i(t) = Vt$ . This is actually the case for DBM patterns. Suppose that  $V$  is so large as to satisfy  $|\dot{b}_i| \ll b_i V^2/D$  and  $|\dot{x}_i| \ll V$ . Then,  $u_i$  may be approximated by a steadily propagating solution

$$u_i(x, y, t) \simeq C_i(t) u_v(x - x_i(t), y - Vt). \quad (6)$$

Therefore,  $F_i(x, t) \equiv U_i(x, Vt, t)$  is expressed in terms of  $(C_j(t), x_j(t))$  as

$$F_i(x, t) \simeq \sum_{j \neq i}^N f(x - x_j(t)) C_j(t), \quad (7)$$

where  $f(x) = u_v(x, Vt)$ .

The time-development of the  $i$ -th finger will be influenced by  $(C_j, x_j)$  of the other fingers through  $F_i(x, t)$ . We believe that the mutual interaction of the fingers in other systems is also expressed in the form similar to Eq.(7).

Finally, we consider the dynamics of  $(C_i, x_i)$  to complete our model. Because each tip is very narrow and experiences only a weak field  $F_i(x, t)$ , the effect of higher order terms and higher spatial derivatives of  $F_i(x, t)$  may be neglected. Therefore, by noticing the reflection symmetry with respect to  $x_i \rightarrow -x_i$ , their equations may generally be expressed as

$$\frac{dC_i}{dt} = g(C_i) - a(C_i) F_i(x_i), \quad \frac{dx_i}{dt} = -b(C_i) \frac{\partial F_i}{\partial x}(x_i). \quad (8)$$

For a variety of real systems, one may expect that the appearances of fingering patterns are basically independent of the detailed nature of the interaction and the elements. Therefore, we take the following simple forms for  $g(C)$ ,  $a(C)$  and  $b(C)$ :

$$g(C) = \alpha - \gamma C, \quad a, b = \text{constant}. \quad (9)$$

We also assume exponential form for  $f(x)$  to simplify Eq.(7), i.e.,

$$f(x) = e^{-\beta|x|}, \quad (10)$$

which has some advantage in numerical simulations. In Eq.(9),  $a$  and  $b$  are assumed positive, because the interaction between fingers usually suppresses growth and works repulsively.

We incorporate splitting and annihilation processes of fingers by introducing thresholds in the following way. If the mass  $C_i$  exceeds the value  $C_{th}$ , the corresponding element is assumed to split into two units with masses  $(1 + \delta)C_i/2$  and  $(1 - \delta)C_i/2$  which are sitting at the same place immediately after the splitting event. Conversely, if  $C_i$  becomes smaller than zero, the corresponding element is removed from the system. Annihilations of fingers means their being left behind the envelope formed by the growing fingers in the case of DBM. Although we may choose other rules which do not conserve the mass, these rules are simplest ones because of the invariance of the field  $\sum_i f(x - x_i)C_i$ .

After suitable rescaling, our equations finally take the form

$$\frac{dC_i}{dt} = \alpha - \gamma C_i - F_i(x_i), \quad (11a)$$

$$\frac{dx_i}{dt} = -\frac{\partial F_i}{\partial x}(x_i), \quad (11b)$$

where

$$F_i(x) = \sum_{j \neq i}^N e^{-\beta|x-x_j|} C_j. \quad (12)$$

These equations must be supplemented with the following rules:

$$C_i > 2 \rightarrow \begin{array}{l} \text{The } i\text{-th element splits into two elements } (1 + \delta, x_i) \\ \text{and } (1 - \delta, x_i) \text{ and } N \text{ increases by one.} \end{array} \quad (13a)$$

$$C_i \leq 0 \rightarrow \begin{array}{l} \text{The } i\text{-th element is removed and } N \text{ decreases by} \\ \text{one.} \end{array} \quad (13b)$$

The parameters  $\alpha$  and  $\gamma$  characterize the nature of the individual element and  $\beta^{-1}$  gives the range of interaction;  $\delta$  indicates anisotropy of splitting.

The above set of equations and rules constitute our basic model. In the present paper, we shall confine our investigation to the case  $\delta = 0$ .

We assume that the system is extended transversally from  $x = 0$  to  $L$  and satisfies periodic boundary condition. Then Eq.(12) is rewritten in the form

$$F_i(x) = \sum_j^N \left[ e^{-\beta|x-x_j|} + \frac{2}{e^{\beta L} - 1} \cosh \beta(x - x_j) \right] C_j - C_i. \quad (14)$$

As  $t \rightarrow \infty$ , the system will tend to settle in a statistical stationarity as a result of the balance between creation and annihilation of the elements.

### 3 Turbulent states and related structures

To examine the system behavior, we begin with the case  $\gamma = 0$ . Figure 1 shows a phase diagram obtained from numerical simulations for transversal system size  $L = 20$ . Turbulent states appear at large  $\alpha$  and  $\beta$  as shown in Fig.2. For sufficiently small  $\alpha$  and  $\beta$  under fixed  $L$ , in contrast, the final state is such that all elements except one are annihilated, although the parameter region corresponding to such a state vanishes as  $L \rightarrow \infty$ .

We introduce average density  $\rho$  and interval  $\tau$  of splitting to characterize the turbulent state. They are defined by

$$\rho \equiv \frac{\langle \sum_i C_i \rangle}{L}, \quad (15a)$$

$$\tau \equiv \frac{\langle \sum_i C_i \rangle}{\langle \frac{d}{dt} N_{split} \rangle}, \quad (15b)$$

where  $dN_{split}(t)/dt$  is the frequency of splitting and  $\langle \cdot \rangle$  represents a long time average.

We found that the distribution function of  $C_i$  has a peak near  $C_i = 1$ . This occurs for the reason that the elements are produced at  $C_i = 1$ , so that  $\rho^{-1}$  gives approximately the mean spacing  $l \equiv L/N$  between elements.  $\rho$  behaves like  $\rho = \beta r(\alpha)$  as shown in Fig.3.  $r(\alpha)$  increases with  $\alpha$  approaching  $\alpha/2$ , because from Eqs.(11) and (14) we have  $dC_i/dt = \alpha - 2\rho/\beta + O(1)$  in the limit of  $\alpha \rightarrow \infty$  under fixed  $\alpha\beta$ .

Equations (11a) and (11b) are also rewritten in terms of “free energy”  $H$ :

$$\frac{dC_i}{dt} = -\frac{\partial H}{\partial C_i}, \quad C_i \frac{dx_i}{dt} = -\frac{\partial H}{\partial x_i}, \quad (16)$$

where

$$H \equiv \sum_i (-\alpha C_i + \frac{1}{2}\gamma C_i^2) + \frac{1}{2} \sum_{i \neq j} e^{-\beta|x_i-x_j|} C_i C_j.$$

Each splitting adds  $1 + \gamma$  to  $H$ , while annihilation does not change  $H$ . Therefore, the time development of  $H$  is governed by the equation

$$\frac{dH}{dt} = - \sum_i D_i + (1 + \gamma) \frac{dN_{split}}{dt}, \quad (17)$$

where

$$D_i \equiv \left( \frac{\partial H}{\partial C_i} \right)^2 + \frac{1}{C_i} \left( \frac{\partial H}{\partial x_i} \right)^2 = (F_i - \alpha - \gamma C_i)^2 + C_i \left( \frac{\partial F_i}{\partial x_i} \right)^2 \geq 0. \quad (18)$$

$\sum_i D_i$  vanishes in the stationary state. We may thus regard  $\sum_i D_i$  as an indicator of disorder. In statistical stationarity, the long-time average of  $dH/dt$  vanishes, so that

$$\left\langle \frac{d}{dt} N_{split} \right\rangle = \frac{1}{1 + \gamma} \left\langle \sum_i D_i \right\rangle. \quad (19)$$

This equation may be interpreted as a balance between the frequency of splitting and the disorder of the system.

The behavior of  $\tau$  obtained from our numerical simulations is described in Fig.1 with contour lines. As  $\alpha$  increases under fixed  $\alpha\beta$ ,  $\tau$  decreases and saturates to a constant. In this limit, the space-time pattern becomes fractal-like as shown in Fig.4. This is not surprising because the range of interaction becomes infinitely long in this limit which is similar to the case of DLA. The wavenumber spectra of the density  $\rho(x) \equiv \sum_i C_i \delta(x - x_i)$  for some different parameter values are illustrated in Fig.5. As we increase  $\alpha$ , the spectrum gives rise to a hump in the intermediate wave numbers and exhibits a power-law decay at large wave numbers. We note that such a change of structure does not reflect in  $\rho$  nor  $\tau$ .

When  $\beta$  is sufficiently small, homogeneous turbulent state changes into a tree-like structure as shown in Fig.6, where the elements move and split in small groups. We may find the number of trees  $n_T$  by counting those spaces  $l_i$  between neighboring elements larger than the mean spacing  $l$ . Then the spacing  $l_T$  and the width  $W$  for the trees are defined by

$$l_T \equiv \frac{L}{\langle n_T \rangle}, \quad (20a)$$

$$W \equiv \frac{1}{\langle n_T \rangle} \left\langle \sum_{l_i < l} l_i \right\rangle. \quad (20b)$$

These definitions are useful only if  $W/l_T$  is sufficiently small.  $l_T$  behaves like  $\beta l_T = h(\alpha)$  similarly to the mean spacing  $l$  as implied from Fig.7. Note that  $l_T/l$  gives the average number of elements per tree and increases with  $\alpha$ .

In the parameter region under consideration, stable periodic structures like those in Figs.8 and 9 easily appear. They become less probable for larger  $L$ . However, they are found to be stable up to sufficiently large  $L$ . They are roughly classified into two groups according to whether the trees propagate or not. Propagating trees appear mainly at small  $\alpha$ , which are composed of relatively small number of elements. We may regard such a tree as a unit with many internal degrees of freedom. As we show in the next section, simple stationary periodic states are unstable if  $\gamma = 0$ . The stable periodic structures imply that the grouping of elements into small assemblies tends to stabilize the pattern.

## 4 Stability of stationary states and STI

We now consider the case  $\gamma \neq 0$ . Eqs.(11a) and (11b) admit a family of stationary solutions. They represent the states in which the elements have the same mass  $C_s$  and regularly spaced with period  $l_s \equiv L/N$ , where

$$C_s \equiv \frac{\alpha}{\gamma + \tilde{F}}, \quad (21a)$$

$$\tilde{F} \equiv \frac{2}{e^{\beta l_s} - 1}. \quad (21b)$$

Note that the value of  $l_s$  is limited by the condition  $0 < C_s \leq 2$ .

In order to study the condition for stability of these stationary states, let  $(C_j, x_j)$  be disturbed from  $(C_s, l_s j)$  slightly, and put  $(C_j, x_j) = (C_s, l_s j) + (\delta C, \delta x)e^{\lambda t + i q j}$  and  $q = \pi/m$  ( $m = 1, 2, \dots$ ). From linearized equations for  $\delta C$  and  $\delta x$ , we obtain an equation for the eigenvalues  $\lambda$  as

$$\lambda \begin{pmatrix} \delta C \\ C_s \delta x \end{pmatrix} = - \begin{pmatrix} \gamma + \tilde{F}_C & \tilde{F}_x \\ -C_s \tilde{F}_x & C_s \beta^2 (\tilde{F} - \tilde{F}_C) \end{pmatrix} \begin{pmatrix} \delta C \\ C_s \delta x \end{pmatrix}, \quad (22)$$

where

$$\tilde{F}_C \equiv \frac{\cos q - e^{-\beta l_s}}{\cosh \beta l_s - \cos q} \quad \text{and} \quad \tilde{F}_x \equiv \frac{-i\beta \sin q}{\cosh \beta l_s - \cos q}.$$

The coefficient matrix in Eq.(22) becomes diagonal for the smallest wavelength  $q = \pi$ , so that  $(1, 0)$  gives the eigenvector with eigenvalue  $\lambda_C \equiv$



$-\gamma + 2/(e^{\beta l_s} + 1)$ . The stationary state with period  $l_s$  becomes unstable when  $\lambda_C > 0$ . The state with the largest  $l_s$ , which corresponds to  $C_s = 2$ , is the most stable but still loses stability at  $\gamma = \gamma_s$ , where

$$\gamma_s \equiv \frac{1}{4}(\alpha + 4 - \sqrt{\alpha^2 + 16}). \quad (23)$$

Thus, all stationary states are unstable for  $\gamma < \gamma_s$ .

From our numerical simulations, the system is found to exhibit turbulent behavior for  $\gamma < \gamma_s$ . When  $\gamma$  exceeds  $\gamma_s$ , the turbulent behavior persists up to a certain value of  $\gamma$  (denoted as  $\gamma_c$ ). Near and below  $\gamma_c$ , the system behavior is characterized by spatio-temporal intermittency (STI), and its typical behavior is shown in Fig.10. We investigated frequency spectra of the field  $\Psi(x, t) \equiv \frac{2}{\beta} \sum_j e^{-\beta|x-x_j|} C_j$  and the size distributions of laminar domains. They are illustrated in Figs.11 and 12, respectively, where we define that a given element is in the laminar phase if  $D_i$  of Eq.(18) is less than  $10^{-4}$ . It is seen that, as the transition point  $\gamma_c$  is approached, the frequency spectrum of  $\Psi(x, t)$  comes to obey a power law. Similarly, the size distribution of the laminar domains also changes from exponential-like behavior to power-law behavior. In Fig.13, we plot  $\rho$  and  $\tau^{-1}$  against  $\gamma$  under fixed  $\alpha$  and  $\beta$ . The figure suggests that  $\tau^{-1}$  approaches zero like  $\tau^{-1} \propto \sqrt{\gamma_c - \gamma}$ . These results are consistent with the STI found in coupled map lattices[9, 5] and also with experiments on directional viscous fingering[12].

## 5 Discussions

In introducing our model in section 2, we assumed that the tip of each finger is well localized, which justifies (i) that the field  $F_i$  of Eq.(7) is sufficiently small and (ii) that  $F_i$  is a superposition of the fields  $u_j$  of the other fingers. The above assumption will not always hold for real fingers. Indeed, the dimension of the tips is nearly the same as the distance between fingers as is seen in the many experiments on viscous fingering and crystal growth. However, if the equation corresponding to Eq.(1) is free from nonlinear terms as is the case of the phase field model[10, 4] for crystal growth, property(ii) is strictly correct and (i) also holds roughly because the field produced by the other fingers will decay through diffusion. Therefore, we believe that our model remains qualitatively.

For such patterns as fat fingers, the dynamics of the internal degrees of freedom could be more important. However, improving the model in this point may cause the problem of coupling between internal degrees of freedom

and splitting processes. In our model, the problem of splitting processes reappears in a higher stage where it becomes more natural to regard each tree as a basic unit.

We derive a phenomenological set of equations in (8) in relation to the dynamics of the bacterial density  $b(\mathbf{x}, t)$ . In order to make a more precise characterization of the individual elements, a systematic method of reduction from real systems to a model system would be needed.

Although without detailed report here, we also carried out numerical simulations using the logistic form  $g(C) = (\alpha - \gamma C)C$  and  $a(C) \propto C$  in place of Eq.(9). In that case, no annihilation occurs so that rule (13b) becomes irrelevant. Still we found qualitatively the same types of behavior as those reported in the present paper. This implies that the decay of the elements is not an essential factor to such behavior.

The relation in Eq.(19) implies that the system becomes more disordered when splitting becomes more frequent. It is, however, a future problem to predict theoretically the degree of disorder which determines the interval  $\tau$  of splitting.

## 6 Acknowledgments

The author would like to acknowledge Y.Kuramoto, T.Mizuguchi, N.Nakagawa and other members of Nonlinear Dynamics group in Kyoto University for valuable discussions.

## Appendix A

If  $\sum_i |\nabla u_i|^2 \simeq |\sum_i \nabla u_i|^2$  in Eqs.(2) and (3), then  $u(\mathbf{x}, t)$  may be approximated with  $u(\mathbf{x}, t) \simeq \sum_i u_i(\mathbf{x}, t)$ . In order to examine whether this is true, we consider the field produced by a typical tip moving with a constant speed  $\mathbf{V}$ .

From Eq.(1) rewritten with a comoving frame  $\mathbf{r} = \mathbf{x} - \mathbf{V}t$ , the nutrient concentration outside the tip obeys the equation  $D \Delta n + \mathbf{V} \cdot \nabla n = 0$ . Therefore, the solution of Eq.(1) approaching a constant  $n_0$  at infinity is expanded in terms of the modified Bessel functions  $K_m(z) \equiv \frac{\pi^i}{2} e^{m\pi i/2} H_m^{(1)}(iz)$ ,  $m = 0, 1, 2, \dots$ , i.e.,

$$n(\mathbf{r}) = n_0 e^{-u(\mathbf{r})} = n_0 \left( 1 - e^{-\frac{\mathbf{V} \cdot \mathbf{r}}{2D}} \sum_{m=0}^{\infty} P_m(\theta) K_m\left(\frac{Vr}{2D}\right) \right), \quad (24)$$

outside the tip, where

$$P_m(\theta) = A_m \cos m\theta + B_m \sin m\theta, \quad \mathbf{r} \cdot \mathbf{V} = rV \cos \theta.$$

$A_m$  and  $B_m$  are constants which are determined from the matching of the above  $n(\mathbf{r})$  inside the tip.

The nutrient concentration  $n(\mathbf{r})$  in Eq.(24) must be positive finite outside the tip. Since  $K_m(x)$  diverge like  $K_0(x) \simeq -\log(x/2)$  and  $K_{m \neq 0}(x) \simeq x^{-m}$  as  $x \rightarrow 0$ , we have  $P_0 \sim O((-\log V\epsilon/2D)^{-1})$  and  $P_{m \neq 0} \sim O((V\epsilon/2D)^m)$ , where  $\epsilon$  is the linear size of the tip region. Therefore, by the assumption that the tip region of each finger is sufficiently localized, the terms of nonvanishing  $m$  may be neglected, thus leading to

$$u(\mathbf{r}) \simeq CK_0\left(\frac{Vr}{2D}\right)e^{-\frac{\mathbf{V}\cdot\mathbf{r}}{2D}} \ll 1 \quad (25)$$

far from the tip, i.e.,  $r \gg \epsilon$ . Here we have used the notation  $C$  for the constant  $P_0(\theta)$ .

When  $u_i \ll 1$ , which is true except near the  $i$ -th tip, the above condition is satisfied because

$$\frac{|\nabla u|^2 - \sum_i |\nabla u_i|^2}{|\Delta u|} \sim \frac{\sum_{i \neq j} u_i u_j}{\sum_i u_i} \ll 1. \quad (26)$$

Therefore, we have  $u(\mathbf{x}, t) \simeq \sum_i u_i(\mathbf{x}, t)$  as expected.

## References

- [1] A.Arnéodo, Y.Couder, G.Grasseau, V.Hakim and M.Raubaud  
Phys.Rev.Lett. 63(1989) 984.
- [2] D.Bensimon, L.P.Kadanoff, S.Lang, B.I.Shraiman and C.Tang  
Rev.Mod.Phys. 58(1986) 977.
- [3] E.Ben-Jacob, O.Schochet, A.Tenenbaum, I.Cohen,  
A.Czirók and T Vicsek  
Nature 368(1994) 46.
- [4] G.Caginalp and P.Fife  
Phys.Rev.B 33(1986) 7792

- [5] H.Cháte and P.Manneville  
Physica D 32(1988) 409.
- [6] H.Fujikawa and M.Matsushita  
J.Phys.Soc.Jpn. 60(1991) 88.
- [7] D.Grier, E.Ben-Jacob, R.Clarke and L.M.Sander  
Phys.Rev.Lett. 56(1986) 1264.
- [8] H.Honjo and S.Ohta  
Phys.Rev.A 45(1992) R8332.
- [9] K.Kaneko  
Prog.Theor.Phys. 74(1985) 1033.
- [10] R.Kobayashi  
Physica D 63(1993) 410.
- [11] T.Matsuyama and M.Matsushita  
Critical Reviews in Microbiology 19(1993) 117.
- [12] S.Michalland, M.Rabaud and Y.Couder  
Europhys.Lett. 22(1993) 17.
- [13] M.Ohgiwari, M.Matsushita and T.Matsuyama  
J.Phys.Soc.Jpn. 61(1992) 816.
- [14] M.Rabaud, S.Michalland and Y.Couder  
Phys.Rev.Lett. 64(1990) 184.
- [15] Y.Saito, C.Mitsbah, H.Müller-Krumbhaar, T.Ueta and M.Uwaha  
Formation, Dynamics and Statistics of Patterns Vol.1 236 edited by  
K.Kawasaki, M.Suzuki and A.Onuki, (World Scientific, 1990).
- [16] H.Sakaguchi  
Prog.Theor.Phys. 91(1994) 1045.
- [17] Y.Sawada, A.Dougherty and J.P.Gollub  
Phys.Rev.Lett. 56(1986) 1260.

- [18] J.Wakita, K.Komatsu, A.Nakahara, T.Matsuyama and M.Matsushita  
J.Phys.Soc.Jpn. 63(1994) 1205.
- [19] T.A.Witten and L.M.Sander  
Phys.Rev.B 27(1983) 5686.

## Figure Captions

- Figure 1  
Phase diagram for the present model system with  $\gamma = 0$  and transversal system size  $L = 20$ .
- Figure 2  
Space-time pattern obtained for  $\alpha = \beta = 1$ ,  $\gamma = 0$  and  $L = 20$  over the time interval of  $T = 75$ . The size of  $C_i$  is indicated by the density of dots.
- Figure 3  
Average density  $\rho$  in a turbulent state obtained for  $\gamma = 0$ .
- Figure 4  
Space-time pattern obtained for  $\alpha = 1000$ ,  $\beta = 0.01$ ,  $\gamma = 0$  and  $L = 20$  over the time interval of  $T = 75$ .
- Figure 5  
Wavenumber spectra  $S(k)$  of the density  $\rho$  (for definition, see the text), where  $\gamma = 0$  and  $\alpha\beta = 20$ .
- Figure 6  
Space-time pattern obtained for  $\alpha = 50$ ,  $\beta = 0.03$ ,  $\gamma = 0$  and  $L = 50$  over the time interval of  $T = 75$ .
- Figure 7  
Behavior of spacing  $l_T$  between trees obtained for  $\gamma = 0$  and  $L = 100$ . (a)  $\beta l_T$  and  $W/l_T$  plotted against  $\beta$ . (b) the average of  $\beta l_T$  plotted against  $\alpha$ ;  $\beta l$  is also plotted for comparison's sake.
- Figure 8  
Space-time pattern obtained for  $\alpha = 4.8$ ,  $\beta = 0.1$ ,  $\gamma = 0$  and  $L = 50$  over the time interval of  $T = 75$ .
- Figure 9  
Space-time pattern obtained for  $\alpha = 0.2$ ,  $\beta = 0.4$ ,  $\gamma = 0$  and  $L = 50$  over the time interval of  $T = 75$ .

- Figure 10  
Space-time pattern obtained for  $\alpha = \beta = 1$ ,  $\gamma = 0.275$  and  $L = 100$  over the time interval of  $T = 150$ .
- Figure 11  
Frequency spectra  $S(\omega)$  of the field  $\Psi$  (for definition, see the text) obtained for  $\alpha = \beta = 1$  and  $L = 100$ .
- Figure 12  
The number of laminar domains  $N(w)$  is plotted as a function of domain size  $w$ , where  $\alpha = \beta = 1$ ,  $L = 1000$  and (left)  $\gamma = 0.26$  with linear-log plots / (right)  $\gamma = 0.28$  with log-log plots. The right figure was produced from the data over the time interval of 10000 after a long transient of 15000.
- Figure 13  
Change of the average density  $\rho$  and the interval  $\tau$  of splitting with increasing  $\gamma$ , where  $\alpha = \beta = 1$  and  $L = 100$ ;  $\gamma_c$  is evaluated to be  $\gamma_c \simeq 0.28 \pm 0.05$ .

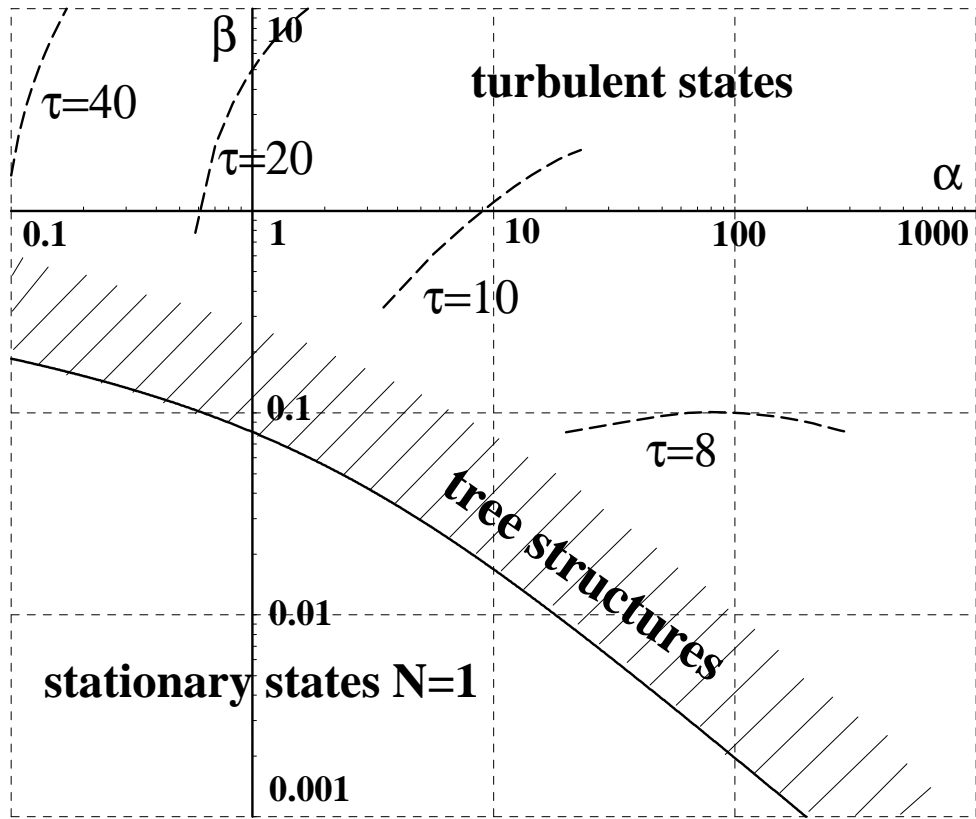


Figure 1

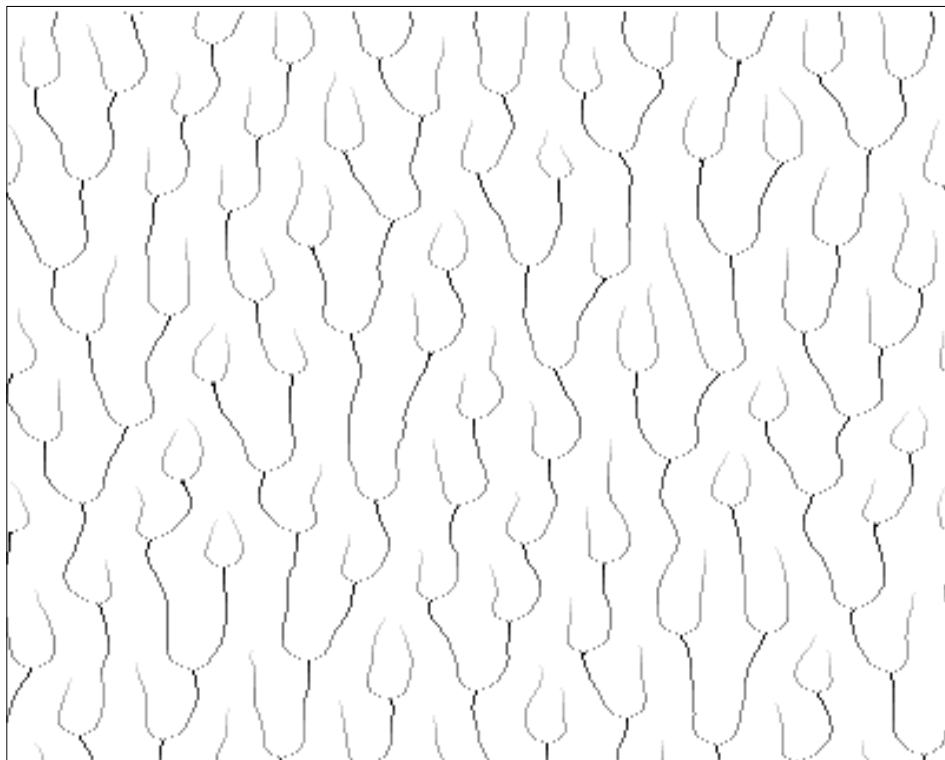


Figure 2



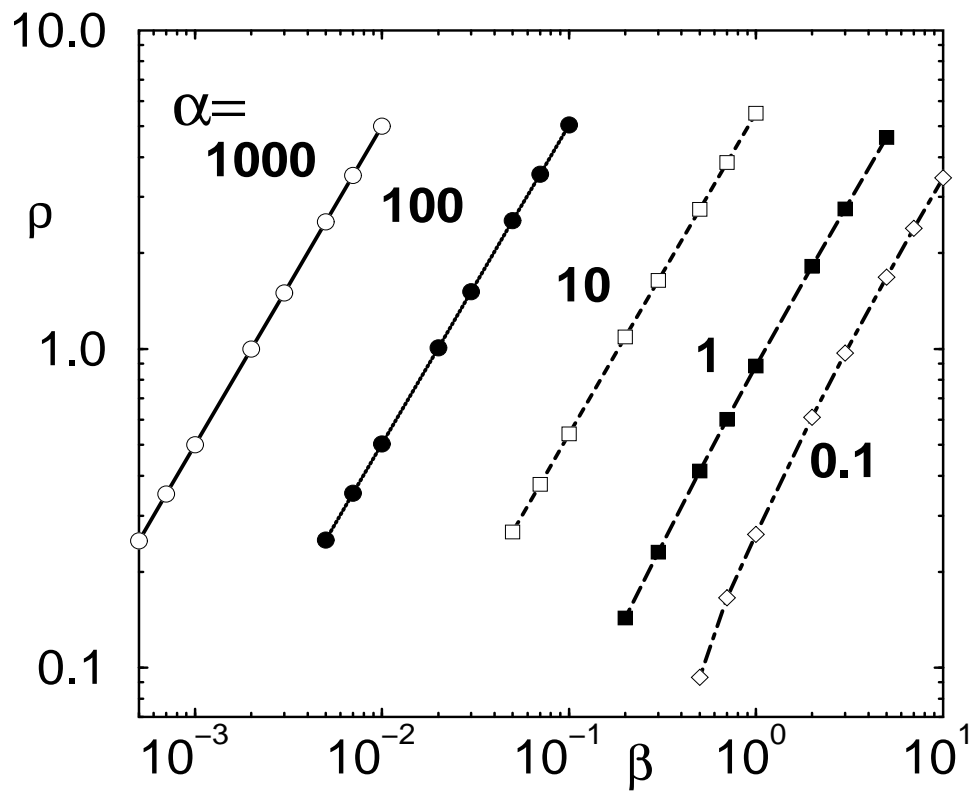


Figure 3

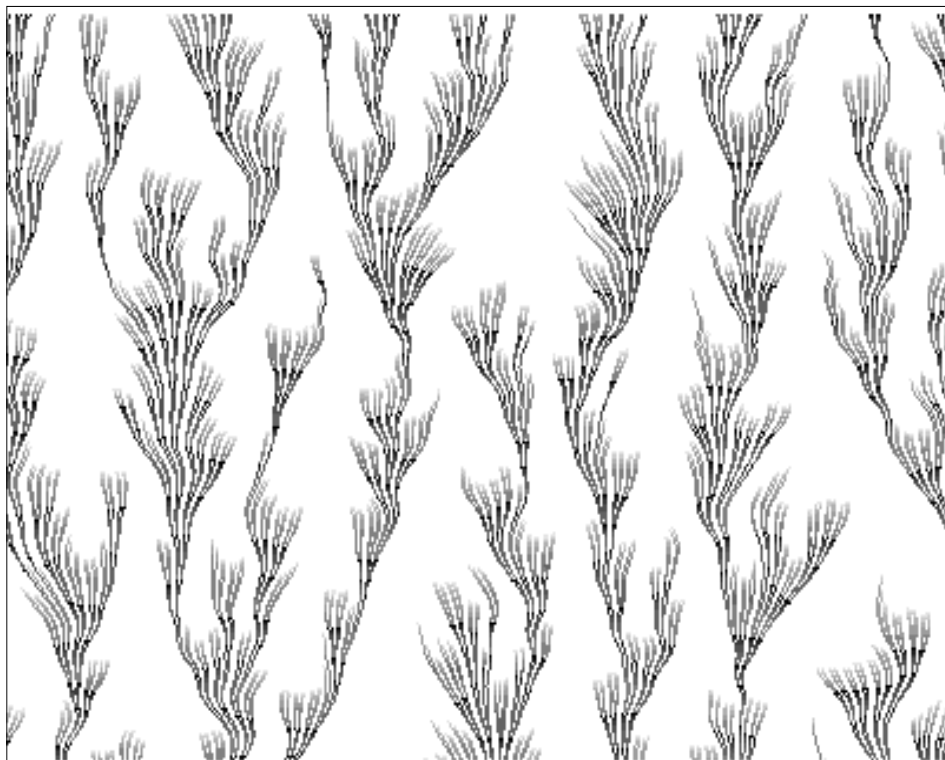


Figure 4

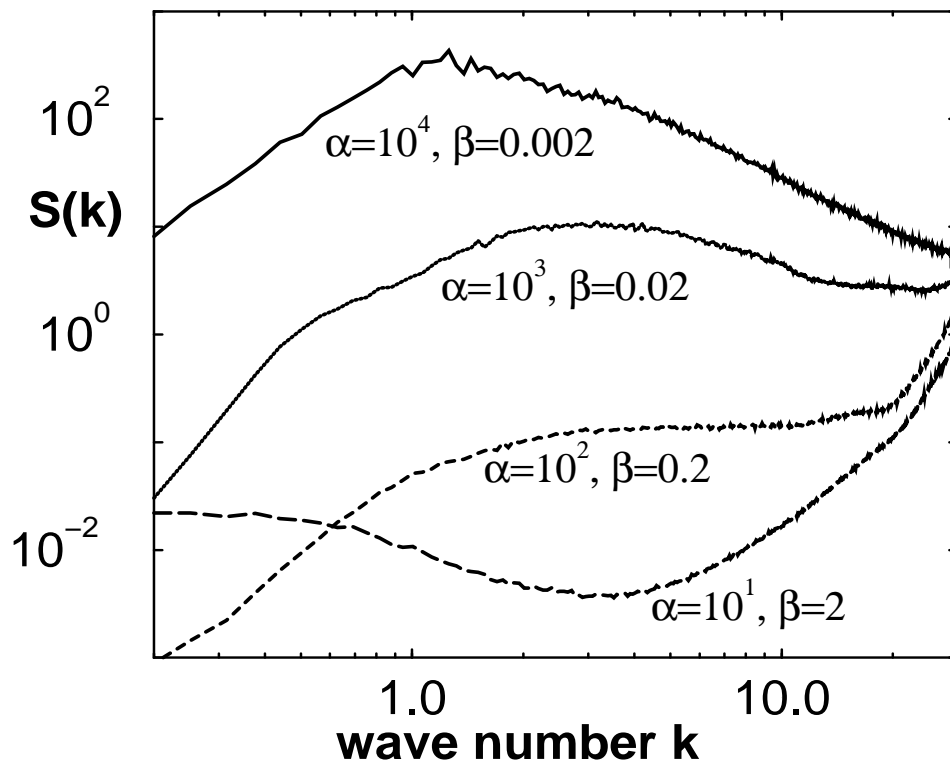


Figure 5

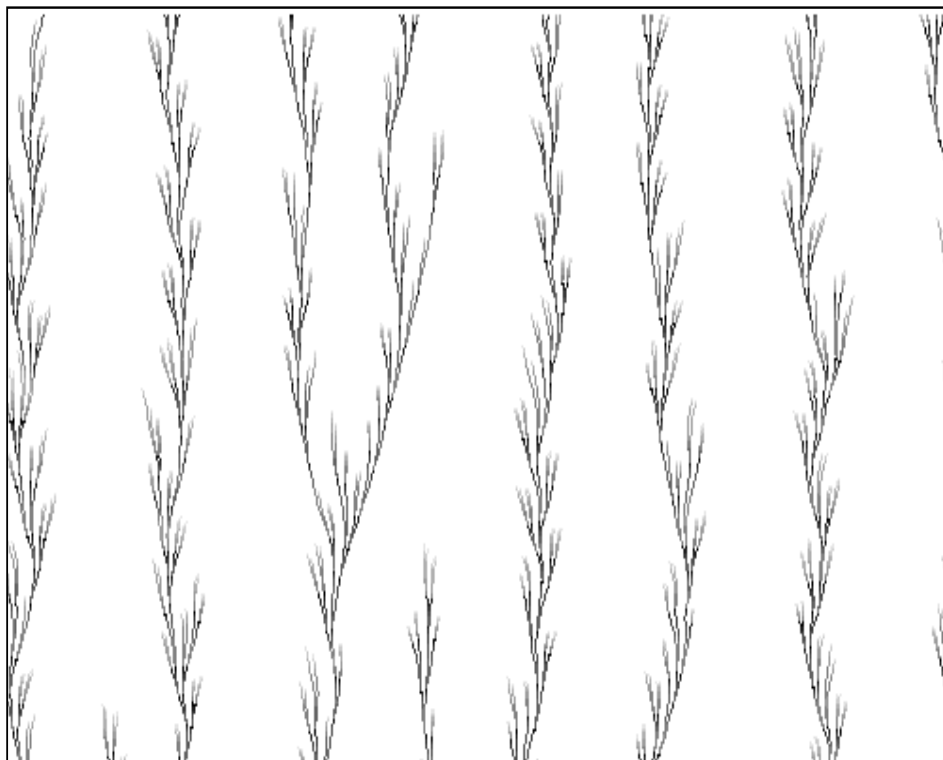
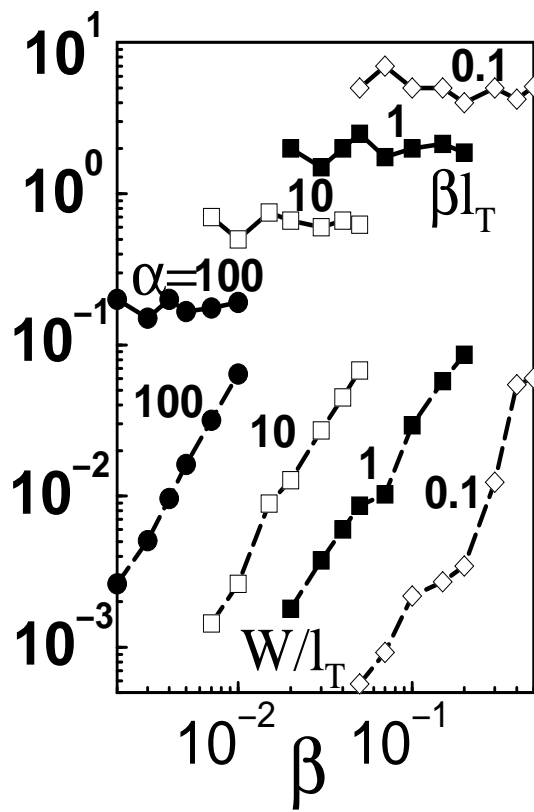
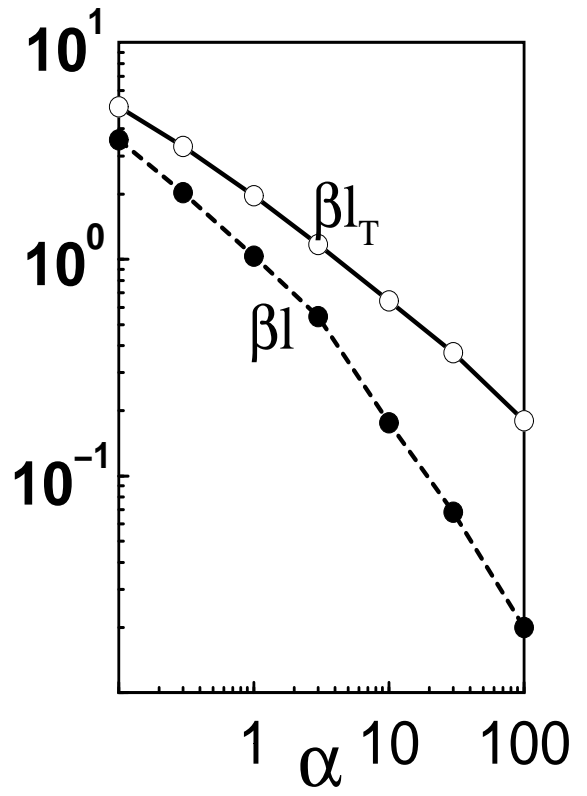


Figure 6



(a)



(b)

Figure 7

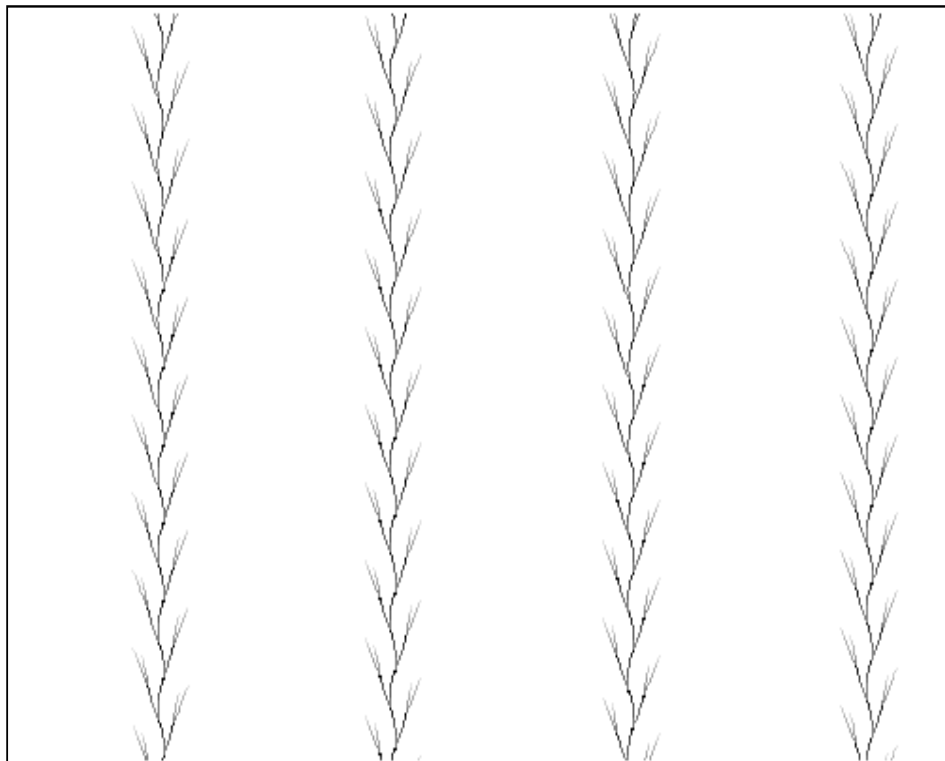


Figure 8

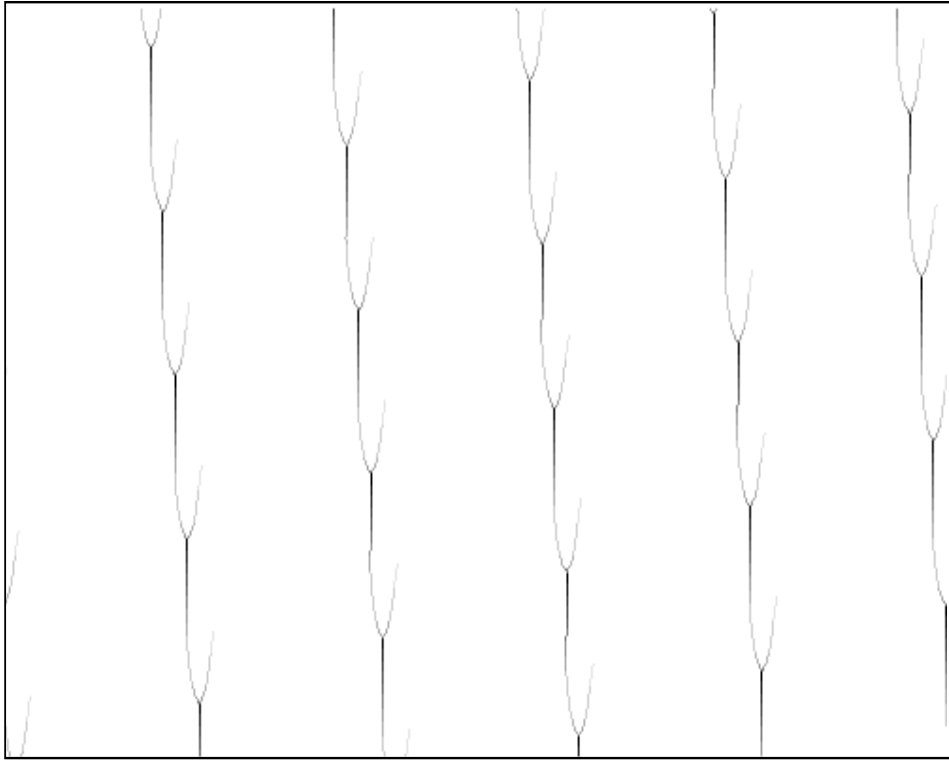


Figure 9

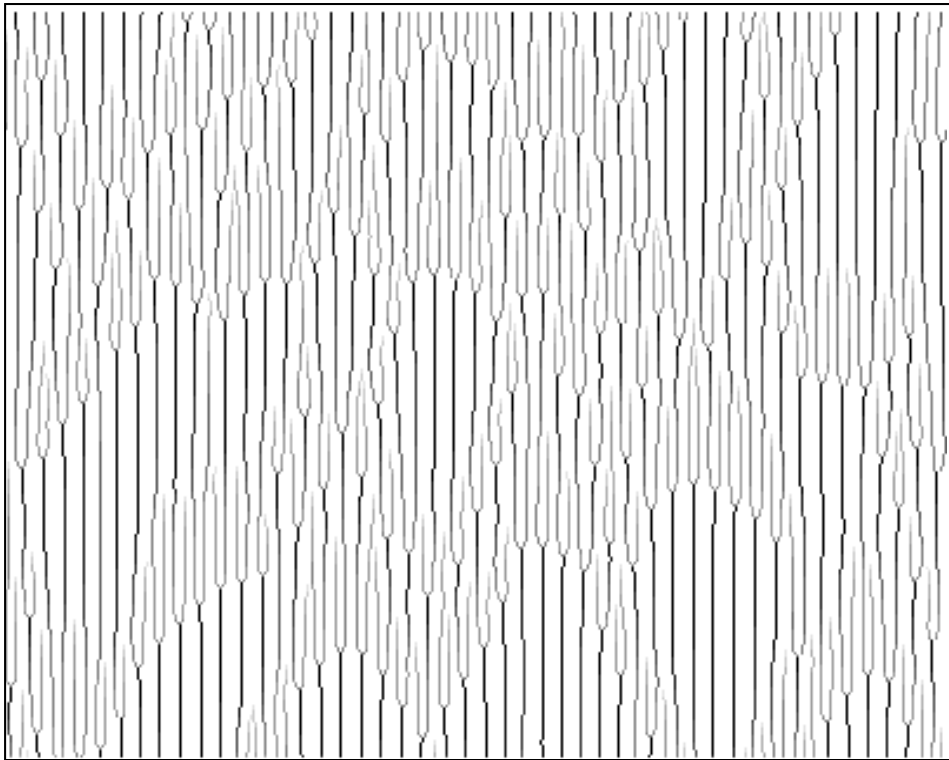


Figure 10

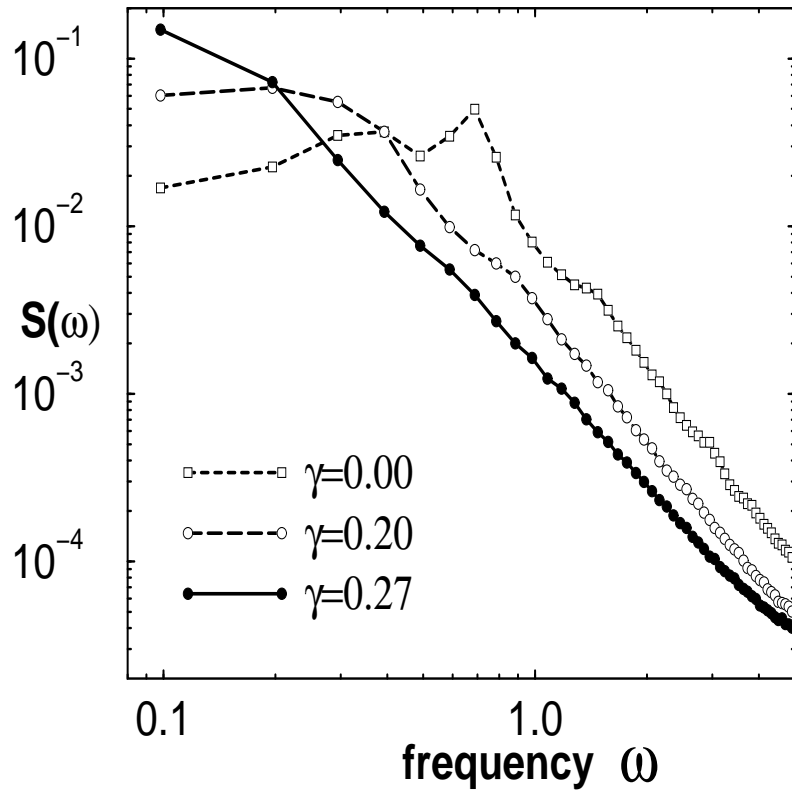


Figure 11

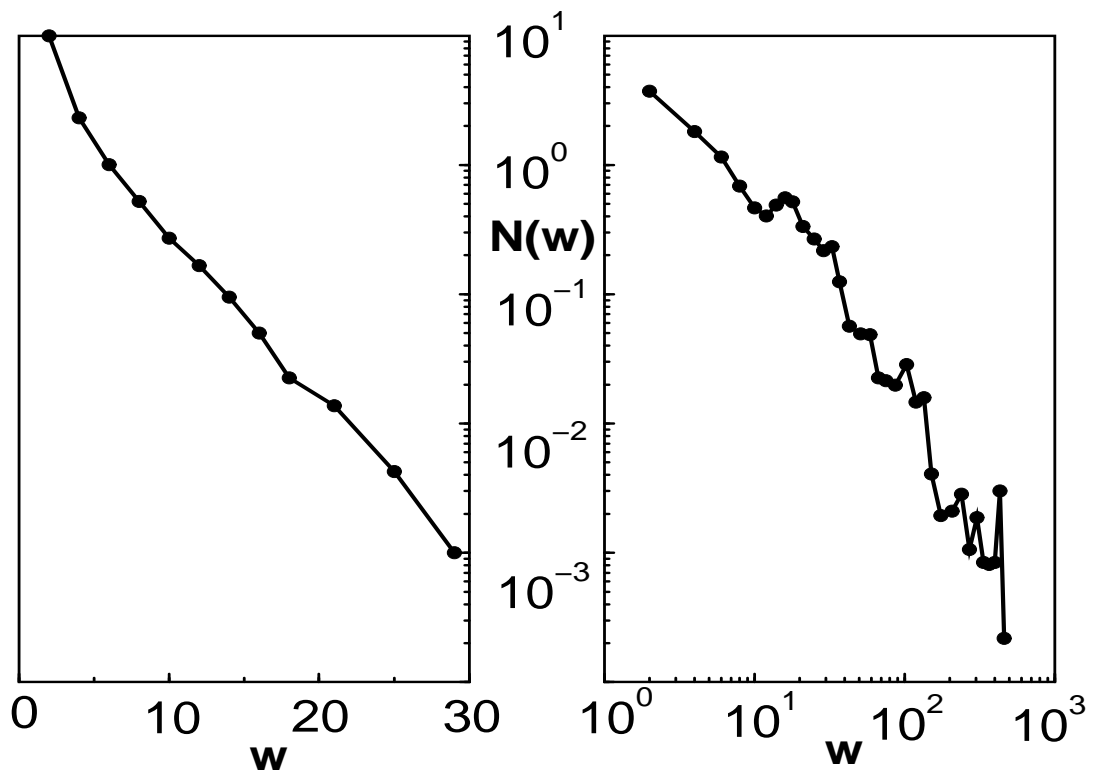


Figure 12

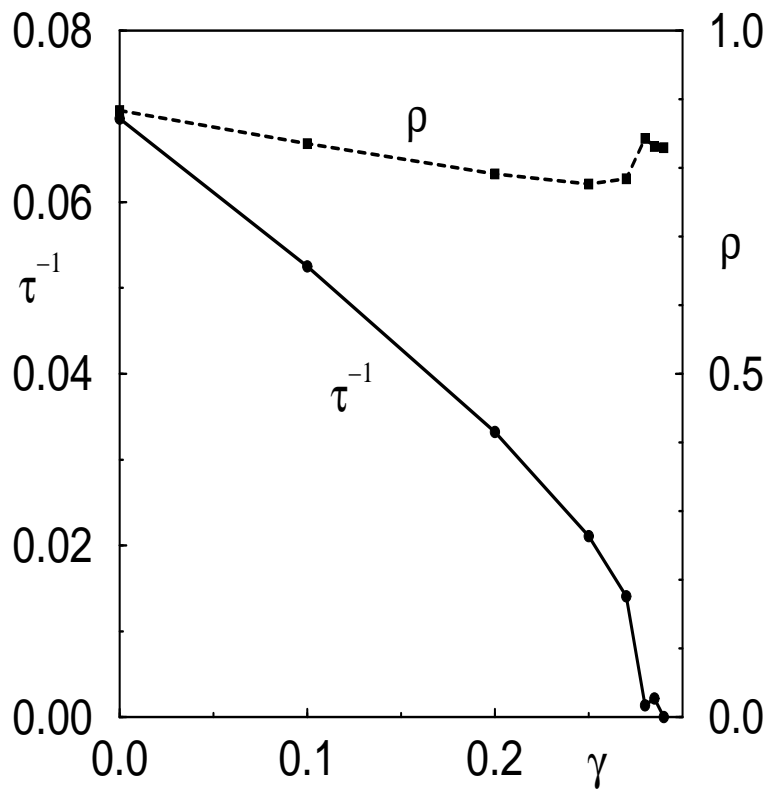


Figure 13